https://doi.org/10.5194/egusphere-2024-1913
Preprint. Discussion started: 2 September 2024

Title:

Brief communication: Morphometric control on the frequency of snow avalanches on the left bank slope of the Tongquan River, southeastern Tibetan Plateau, China

Hong Wen [a], Zuqi Xia [a], Xiaoyan Shu [b], Dong Wang [c], Chunwei Sun [a], Qingshui Qiu [a], Xiaoning Li [d *]

Affiliations:

[a] *School of Architecture and Civil Engineering, Xihua University, Chengdu 610039, China*

[b] *Faculty of Geosciences and Environmental Engineering, Southwest Jiaotong University, Chengdu 611756, China*

[c] *China Railway First Survey and Design Institute Group Co. Ltd，Xi'an 710043, China*

[d] *School of Emergency Management, Xihua University, Chengdu 610039, China*

***Corresponding author**

Name: Xiaoning Li

Email: swustlxn@126.com

Affiliation: School of Emergency Management, Xihua University

Address: 999# Jin Zhou Rd. Jinniu District, Chengdu 610039, Sichuan Province, China

https://doi.org/10.5194/egusphere-2024-1913
Preprint. Discussion started: 2 September 2024

Abstract

Understanding the frequency of occurrence and mechanisms controlling snow avalanches (hereafter referred to as avalanches) is crucial for effective disaster prevention and mitigation, especially in the context of climate warming. In this study, the topographic features and historical activities within the four avalanche paths on the left bank slope of the Tongquan River are meticulously analysed through a comprehensive approach that combines field investigations, long-term remote sensing interpretation, and spatial analysis. Additionally, the morphometric controls on avalanche frequency are further investigated. The results indicate that the occurrence frequencies of the four avalanche paths on the same slope, despite having nearly identical macrometeorological and climatic conditions, are not uniform. This variation depends on morphometric factors, such as the size of the starting zone and slope orientation.

Keywords: snow avalanche, avalanche frequency, morphometric control, remote sensing, southeastern Tibetan Plateau

https://doi.org/10.5194/egusphere-2024-1913
Preprint. Discussion started: 2 September 2024

1. Introduction

Snow avalanches (hereafter called avalanches) are rapid gravity-driven masses of snow that move down mountain slopes, posing significant threats to the safety of residents and infrastructure in snowy mountainous regions (McClung, 2016; Schweizer et al., 2021). Since the mid-20th century, the widespread implementation of avalanche prevention measures has significantly reduced avalanche-related fatalities along roadways and in residential areas worldwide (Schweizer et al., 2021). However, in China, the expansion of human activities and major engineering projects into alpine regions has increased the exposure of people and infrastructure to avalanche threats. On January 17, 2023, an avalanche that occurred on Duoxiongla Mountain in southeastern Tibet buried 17 vehicles on the Linzhi-Motuo Highway and resulted in 28 deaths (Chen et al., 2024). This severe avalanche disaster highlights the inadequate understanding of the frequency of occurrence and mechanisms that form avalanches on the Qinghai-Tibet Plateau. Avalanche development is influenced by terrain features, such as altitude and slope, as well as climatic conditions, such as snowfall and temperature (Schweizer et al., 2003). Although avalanches share common initiation, movement, and accumulation processes (Li et al., 2020; Schweizer et al., 2021), different background conditions present distinct occurrence frequencies and formation mechanisms (Reuter et al., 2022; Wen et al., 2024). As a unique mid-latitude plateau, the Qinghai–Tibet Plateau has avalanches that are similar to those of other avalanche-prone zones but possesses distinctive characteristics due to its unique terrain and climatic conditions (Wen et al., 2024). Previous research has focused mainly on spatial distribution patterns (Caiserman et al., 2022; Laxton and Smith, 2009; Singh et al., 2022; Wen et al., 2022), with limited in-depth studies on the frequency of occurrence and mechanisms of formation of avalanches on the Qinghai–Tibet Plateau. Here, the left bank slope of the Tongquan River in southeastern Tibet, a representative slope with four avalanche paths, is used as the study site. Through detailed field investigations combined with long-term remote sensing interpretation and spatial analysis, in this study, the topographic features of avalanche paths are

https://doi.org/10.5194/egusphere-2024-1913
Preprint. Discussion started: 2 September 2024

meticulously delineated, and historical patterns of avalanche occurrence are identified. Subsequently, the morphometric controls on the frequency of avalanches on this slope are discussed.

2. Data and methodology

2.1 Avalanche paths

The Tongquan River is located on the southern slope of the Boshula Range in southeastern Tibet (Fig. 1a). The Boshula range extends from the Nyenchenthanglha Mountains, connecting to the Gaoligong Mountains in the south, with the mountain massif stretching northwest–southeast (Fig. 1b). The Tongquan River is administratively located in Tongshen village, Duoji township, Bomi County. Starting in November 2018, we conducted ten field investigations in Tongquan Valley. Avalanche path identification in the field was based on deposits at the slope foot and gully. In surveys conducted in summer, avalanche-caused vegetation features, such as prostrate trees, flag trees, and altered vegetation communities, were clearly identifiable. Four avalanche paths were identified on the left bank slope of the Tongquan River, numbered 1 to 4 from north to south (Fig. 1). These avalanches were mainly channeled avalanches that run out below the timberline. Remotely piloted aerial vehicle (RPAV) and remote sensing images were utilized to identify the spatial extent of the avalanche starting zone, track zone, and runout zone. These data were combined with land cover survey results for accurate identification of runout zones.

https://doi.org/10.5194/egusphere-2024-1913
Preprint. Discussion started: 2 September 2024

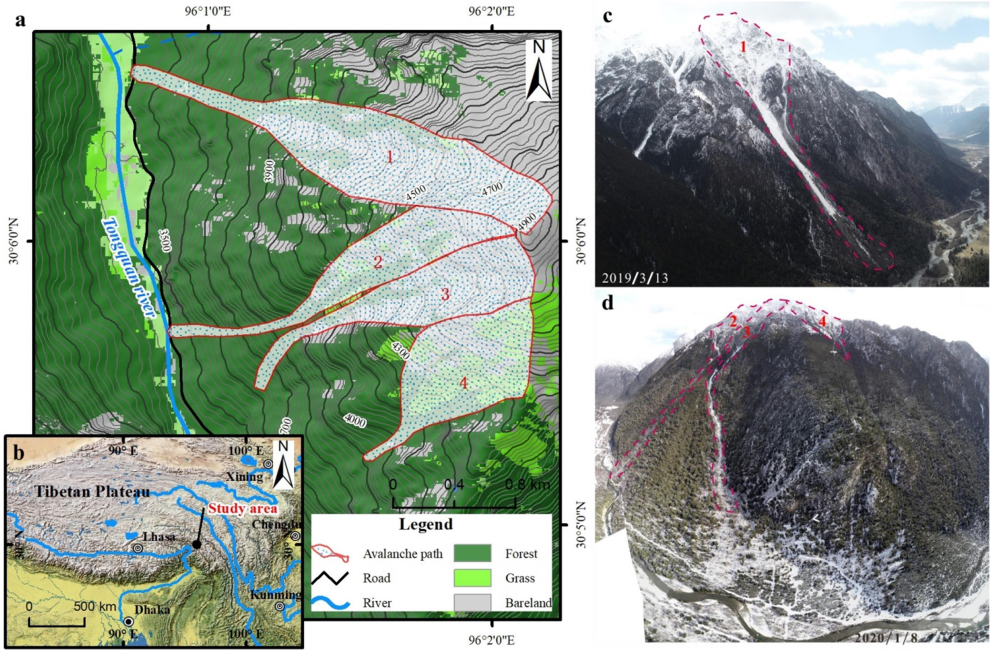

Fig.1 Distribution map and photos of avalanche paths.

a. Avalanche paths distribution map with land cover; b. Location of the study area; c. Photo of avalanche path 1; d. Photo of avalanche path 2, 3 and 4.

2.2 Remote sensing interpretation and spatial analysis

Historical avalanche flow paths within these zones were identified using long-term optical remote sensing interpretation. Data from Landsat 5 (1984-2013) and Landsat 8-9 (2013-present) provided nearly 37 years (1986/1987-20223/2024) of continuous optical remote sensing data. The Landsat satellites have a re-entry period of 16 days; however, the study area is situated in the region in which the 2 orbital paths overlap, resulting in an effective re-entry period of 8 days. After excluding images with more than 30% cloud cover, 194 scenes from Landsat 8-9 and 336 scenes from Landsat 5 were utilized. The interpreted signature focused on the avalanche deposits remaining in the track and runout zones postrelease. Due to collision and compression during avalanche movement, the density and hardness of snow increase, leading to a

https://doi.org/10.5194/egusphere-2024-1913
Preprint. Discussion started: 2 September 2024

slower ablation rate compared to that of undisturbed snow, which often takes 1-2 months to fully ablate. These deposits are generally white, but with image enhancement, they appear blue on remote sensing images, making them easily distinguishable from the surrounding land cover. In the process of interpreting historical avalanche activities, the centre points of the starting zones were taken as the points of initial movement, and the historical avalanche flow paths were plotted along the deposit. Based on this, the successive avalanche runout distances can be further obtained via terrain calculations. The elevation, slope, aspect, surface roughness and other topographic parameters of avalanche paths and subzones (starting zone, track, and runout zone) were extracted for spatial heterogeneity analysis. The Advanced Land Observing Satellite (ALOS) digital elevation model (DEM), with a 12.5-m resolution (https://www.jaxa.jp/) was used to determine the slope angle, slope aspect, surface roughness, and other topographic calculations.

3. Results

3.1 Basic morphometric characteristics of avalanche paths

Through spatial analysis based on a geographic information system (GIS) platform, the main morphometric parameters of these four avalanche paths and their starting zones were obtained, as shown in Table 1. Among these four avalanche paths, Avalanche Path 1 has the largest catchment area and starting zone area, measuring 0.831 km² and 0.726 km², respectively, while Avalanche Path 2 has the smallest catchment area and starting zone area, with areas of 0.401 km² and 0.335 km², respectively. The average slopes of these four avalanche paths are within the 30- to 35-degree range, indicating a high propensity for avalanche occurrence. The average elevation of the starting zones is approximately 4450 m, with Avalanche 3 having the highest elevation of the starting zone, at approximately 4530 m and Avalanche 1 having the lowest, at approximately 4384 m. The average slope of the starting zones is slightly greater than that of each entire path, i.e., within the 35- to 40-degree range. Among these four starting zones, Avalanche 3 has the highest average roughness of 1.334 and the largest standard deviation of 0.196, indicating the greatest surface irregularity; Avalanche 3

https://doi.org/10.5194/egusphere-2024-1913
Preprint. Discussion started: 2 September 2024

111 also exhibits the highest standard deviation for the average curvature, average profile curvature, and average plan
112 curvature, highlighting the most rugged terrain, consistent with the roughness data. In terms of the average curvature,
113 only the starting zone of Avalanche 3 has a negative value, while the starting zone of Avalanche 1 is closest to zero. For
114 the average profile curvature, all four starting zones have negative values, with Avalanche 2 having the smallest value at
115 -0.047. Regarding the average plan curvature, the starting zones of Avalanches 1 and 3 have negative values, whereas
116 the other two zones have positive values.

117 Table 1 Morphometric characteristic parameters of avalanche paths and their starting zones.

Avalanche ID		**1**	**2**	**3**	**4**
Avalanche path	Area (km^2)	0.831	0.401	0.447	0.481
	Length (m)	2497	2137	1845	1404
	Max elevation (m)	4946	4893	4902	4811
	Min elevation (m)	3458	3429	3617	3903
	Relative elevation difference (m)	1488	1464	1285	908
	Average slope (°)	30.8	34.4	34.9	32.9
Starting zone	Area (km^2)	0.726	0.335	0.39	0.441
	Average elevation (m)	4384	4457	4530	4430
	Average slope (°)	36.6	36.7	39.2	36.6
	Average roughness (Std.)	1.282 (0.178)	1.274 (0.139)	1.334 (0.196)	1.268 (0.121)
	Average curvature (Std.)	0.0004 (2.404)	0.121 (2.218)	-0.088 (2.735)	0.039 (1.752)
	Average profile curvature (Std.)	-0.014 (1.42)	-0.047 (1.211)	-0.029 (1.592)	-0.006 (1.066)
	Average plan curvature (Std.)	-0.015 (1.402)	0.074 (1.385)	-0.117 (1.614)	0.032 (1.001)

118 Furthermore, we extracted the aspects of the avalanche starting zones, as depicted in Fig. 2a & b. It is evident that the
119 dominant aspect of Avalanche Path 1's starting zone is markedly different from those of Avalanche Paths 2, 3, and 4.
120 Specifically, the dominant aspect of Avalanche Path 1's starting zone is northwest, accounting for nearly 50% of the
121 aspects. In contrast, the dominant aspects of the starting zones of Avalanche Paths 2, 3, and 4 are southwest, with
122 proportions of 62.69%, 46.55%, and 57.77%, respectively.

https://doi.org/10.5194/egusphere-2024-1913
Preprint. Discussion started: 2 September 2024

3.2 Historical avalanche activity

During multiple field investigations, we observed that the occurrence frequencies of the four avalanches were inconsistent. By analysing optical images from the past 37 years, we recorded 120 historical flow paths within Avalanche Path 1, 26 within Avalanche Path 2, 58 within Avalanche Path 3, and 27 within Avalanche Path 4, as visible in Landsat images, primarily from October to May (Fig. 2c). Figure 2c shows that Avalanche Path 1 has the most frequent historical activity, with the highest frequencies occurring in January and March. Avalanche Path 3 has the second-highest activity frequency. Avalanches along Paths 2 and 4 occur less frequently. In terms of recurrence periods, Avalanche Path 1 exhibits a consistent annual pattern, with avalanches typically occurring 2 to 5 times per year. Avalanche Path 3 has a recurrence period of approximately 4 to 6 years, while avalanches within Paths 2 and 4 occur the least frequently, with no clear recurrence pattern.

https://doi.org/10.5194/egusphere-2024-1913
Preprint. Discussion started: 2 September 2024

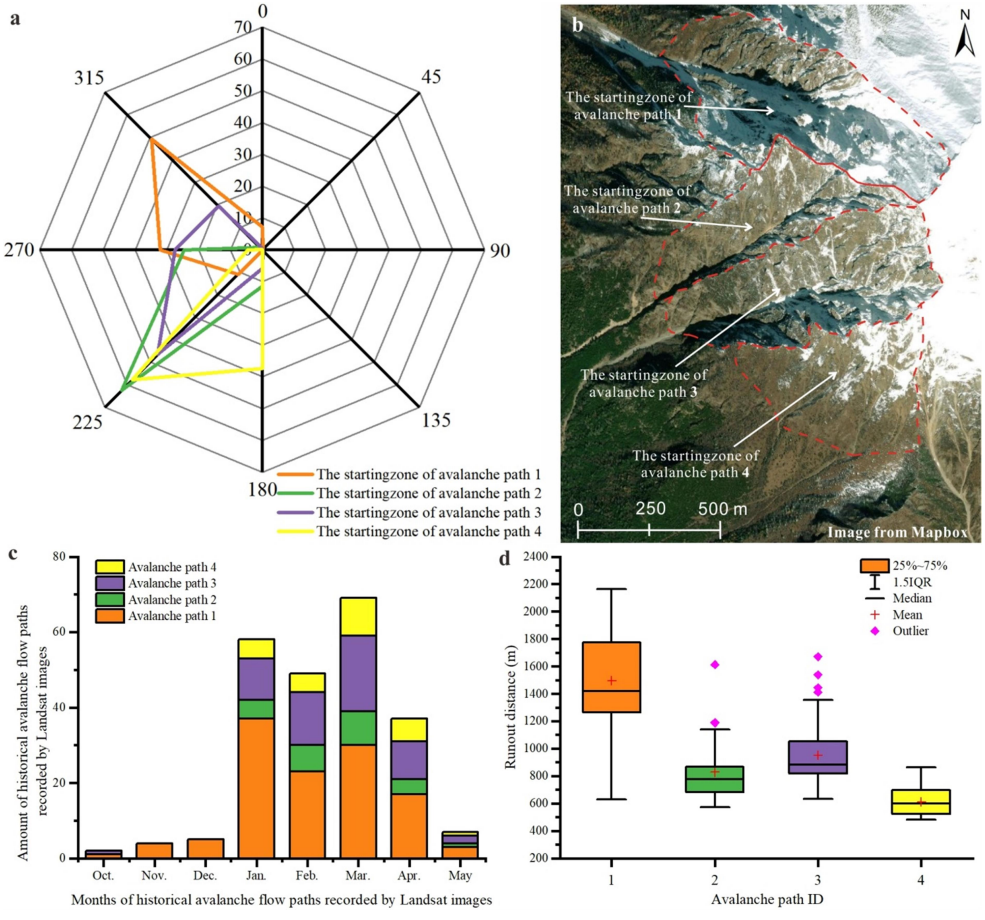

Fig.2 The aspect of the avalanche starting zones and statistical analysis of historical avalanche activity. a. Radar chart of aspect distribution in avalanche starting zones; b. High-Resolution remote sensing images of avalanche starting zones; c. Stacked histogram of avalanche months recorded by Landsat images; d. Boxplot of historical avalanche runout distance.

The historical avalanche runout distances are shown in Fig. 2d. The average historical runout distance of Avalanche Path 1 is 1495 m, with a maximum runout distance of 2161 m. Avalanche Path 2 has an average historical runout distance of 828 m, with a maximum of 1612 m. Avalanche Path 3 has an average historical runout distance of 950 m, with a maximum of 1671 m. Avalanche Path 4 has an average historical runout distance of 610 m, with a maximum of 864 m.

https://doi.org/10.5194/egusphere-2024-1913
Preprint. Discussion started: 2 September 2024

Avalanche Path 1 exhibits both the highest average and maximum runout distances. Additionally, the maximum runout distances of Avalanche Paths 2 and 3 are statistical outliers.

4. Discussion and conclusion

The avalanches along the four paths on this slope do not occur at the same frequency. Studies in other areas have shown that meteorological factors influence avalanche frequency (Hancock et al., 2021; Jomelli et al., 2007; Voiculescu et al., 2016). However, the four paths here are situated on the same slope, where the macroclimatic and meteorological conditions are generally consistent. Therefore, any differences in avalanche frequency are likely due to local topographic variations causing subtle climatic differences. The comparative analysis indicates that Avalanche Path 1, which exhibits frequent activity, is unique primarily in terms of the path area and starting zone area. However, it does not exhibit significant differences in terms of slope, elevation, roughness, or curvature. Further slope orientation analyses reveal that the dominant slope orientation in the starting zone of Avalanche Path 1 is northwest, while the dominant slope orientations in the starting zones of Avalanche Paths 2, 3 and 4 are southwest. The aspect of a slope influences its exposure to sunlight, prevailing wind direction, and path of moisture-laden airflows (Schweizer et al., 2003). These factors affect the distribution of snowfall, the duration of solar radiation on snowpack, the temperature field distribution of snowpack, and the characteristics of snow metamorphism (Alonso-González et al., 2020; Bruland, 2021). Snowfall caused by moist airflow from the Indian Ocean, which is driven by prevailing south winds, tends to accumulate thick snowdrifts on the leeward slopes north of the nearly east–west mountain ridges. These areas become snow accumulation sites, with cornices extending northwards. Cornices are highly unstable and can trigger avalanches when they break and fall (Veilleux et al., 2021; Vogel et al., 2012). Moreover, snow on south-facing sunny slopes receives abundant solar radiation heat, facilitating snowmelt. In contrast, snow on shady slopes receives little to no solar radiation during winter and spring, allowing snow to persist and accumulate. This results in a more abundant source of

https://doi.org/10.5194/egusphere-2024-1913
Preprint. Discussion started: 2 September 2024

material for avalanches. This difference is the primary reason why avalanches are more frequent within Avalanche Path 1 than within the other paths.

Studies in other regions have shown that the spatial distribution of avalanches is controlled by topographic factors, such as valley direction, slope orientation, and relative slope height, while the timing and frequency of avalanches are controlled by the intensity of snowfall, periods of strong winds, and the direction of the prevailing winds (Eckerstorfer and Christiansen, 2011; Laute and Beylich, 2014). Among the starting zones of the four avalanche paths, Avalanche Path 2 has the smallest starting zone, resulting in limited snow storage during the snow season and fewer avalanche occurrences. Avalanche Path 4, with a predominantly southwest and south-facing aspect, receives more solar radiation during the snow season compared to other avalanche paths. Additionally, as a windward slope, it accumulates less snow than the leeward slope of Avalanche Path 1, resulting in fewer avalanches. The starting zone of Avalanche Path 3 has the highest average roughness, indicating that it has the most uneven surface. Snow accumulation on such uneven slopes requires a significant amount of snow to fill irregularities. Overall, macroclimatic and meteorological conditions are not sufficient to explain differences in the frequency of avalanche paths on the same slope, and the topographic conditions of the starting zone, such as the size of the area, slope orientation, and roughness, control the avalanche frequency.

Competing interests

The authors declare that they have no conflict of interest.

Acknowledgments

This study was supported by the National Natural Science Foundation of China (42077271), Central Guidance for Local Science and Technology Development Foundation of China (2023ZYD0155), Open Project of Major Hazard

https://doi.org/10.5194/egusphere-2024-1913
Preprint. Discussion started: 2 September 2024

Measurement and Control Key Laboratory of Sichuan Province (KFKT-2023-06) and the Talent Introduction Project of Xihua University (Z231013). The authors would like to thank the USGS for providing the Landsat images in Open Source.

References

Alonso-González, E., López-Moreno, J. I., Navarro-Serrano, F., Sanmiguel-Vallelado, A., Aznárez-Balta, M., Revuelto, J., and Ceballos, A.: Snowpack sensitivity to temperature, precipitation, and solar radiation variability over an elevational gradient in the Iberian mountains, Atmospheric Research, 243, 104973, https://doi.org/10.1016/j.atmosres.2020.104973, 2020.

Bruland, O.: Snow processes, modeling, and impact. In: Precipitation, Rodrigo-Comino, J. (Ed.), Elsevier, https://doi.org/10.1016/B978-0-12-822699-5.00006-9, 2021.

Caiserman, A., Sidle, R. C., and Gurung, D. R.: Snow Avalanche Frequency Estimation (SAFE): 32 years of monitoring remote avalanche depositional zones in high mountains of Afghanistan, The Cryosphere, 16, 3295-3312, https://doi.org/10.5194/tc-16-3295-2022, 2022.

Chen, N., Li, A., Tian, S., Rahman, M., Huang, N., She, D., Li, Z., and Ding, H.: Characteristics and causes of a catastrophic snow avalanche that occurred on January 17, 2023, in Tibet, Landslides, https://doi.org/10.1007/s10346-023-02205-5, 2024.

Eckerstorfer, M. and Christiansen, H. H.: Topographical and meteorological control on snow avalanching in the Longyearbyen area, central Svalbard 2006-2009, Geomorphology, 134, 186-196, https://doi.org/10.1016/j.geomorph.2011.07.001, 2011.

Hancock, H., Hendrikx, J., Eckerstorfer, M., and Wickström, S.: Synoptic control on snow avalanche activity in central Spitsbergen, The Cryosphere, https://doi.org/10.5194/tc-2021-48, 2021.

Jomelli, V., Delval, C., Grancher, D., Escande, S., Brunstein, D., Hetu, B., Filion, L., and Pech, P.: Probabilistic analysis of recent snow avalanche activity and weather in the French Alps, Cold Regions Science and Technology, 47, 180-192, https://doi.org/10.1016/j.coldregions.2006.08.003, 2007.

Laute, K. and Beylich, A. A.: Morphometric and meteorological controls on recent snow avalanche distribution and activity at hillslopes in steep mountain valleys in western Norway, Geomorphology, 218, 16-34, https://doi.org/10.1016/j.geomorph.2013.06.006, 2014.

Laxton, S. C. and Smith, D. J.: Dendrochronological reconstruction of snow avalanche activity in the Lahul Himalaya, Northern India, Natural Hazards, 49, 459-467, https://doi.org/10.1007/s11069-008-9288-5, 2009.

Li, X. Y., Sovilla, B., Jiang, C. F. F., and Gaume, J.: The mechanical origin of snow avalanche dynamics and flow regime transitions, The Cryosphere, 14, 3381-3398, https://doi.org/10.5194/tc-14-3381-2020, 2020.

McClung, D. M.: Avalanche character and fatalities in the high mountains of Asia, Annals of Glaciology, 57, 114-118, https://doi.org/10.3189/2016AoG71A075, 2016.

https://doi.org/10.5194/egusphere-2024-1913
Preprint. Discussion started: 2 September 2024

216 Reuter, B., Viallon-Galinier, L., Horton, S., van Herwijnen, A., Mayer, S., Hagenmuller, P., and Morin, S.:
217 Characterizing snow instability with avalanche problem types derived from snow cover simulations, Cold Regions
218 Science and Technology, 194, 103462, https://doi.org/10.1016/j.coldregions.2021.103462, 2022.

219 Schweizer, J., Bartelt, P., and van Herwijnen, A.: Snow Avalanches. In: Snow and Ice-Related Hazards, Risks and
220 Disasters, Elsevier, https://doi.org/10.1016/b978-0-12-394849-6.00012-3, 2021.

221 Schweizer, J., Bruce Jamieson, J., and Schneebeli, M.: Snow avalanche formation, Reviews of Geophysics, 41, 1016,
222 https://doi.org/10.1029/2002rg000123, 2003.

223 Singh, K. K., Singh, D. K., Thakur, N. K., Dewali, S. K., Negi, H. S., Snehmani, and Mishra, V. D.: Detection and
224 mapping of snow avalanche debris from Western Himalaya, India using remote sensing satellite images, Geocarto
225 International, 37, 2561-2579, https://doi.org/10.1080/10106049.2020.1762762, 2022.

226 Veilleux, S., Decaulne, A., and Bhiry, N.: Snow cornice and snow avalanche monitoring using automatic time lapse
227 cameras in Tasiapik Valley, Nunavik (Québec) during the winter of 2017–2018, Arctic Science, 7, 798-812,
228 https://doi.org/10.1139/as-2020-0013, 2021.

229 Vogel, S., Eckerstorfer, M., and Christiansen, H. H.: Cornice dynamics and meteorological control at Gruvefjellet,
230 Central Svalbard, The Cryosphere, 6, 157-171, https://doi.org/10.5194/tc-6-157-2012, 2012.

231 Voiculescu, M., Ardelean, F., Torok-Oance, M., and Milian, N.: Topographical Factors, Meteorological Variables and
232 Human Factors in the Control of the Main Snow Avalanche Events in the Fagaras Massif (Southern Carpathians -
233 Romanian Carpathians): Case Studies, Geogr Pol, 89, 47-64, https://doi.org/10.7163/GPol.0045, 2016.

234 Wen, H., Wu, X., Shu, X., Wang, D., Zhao, S., Zhou, G., and Li, X.: Spatial heterogeneity and temporal tendency of
235 channeled snow avalanche activity retrieved from Landsat images in the maritime snow climate of the Parlung Tsangpo
236 catchment, southeastern Tibet, Cold Regions Science and Technology, 223, 104206,
237 https://doi.org/10.1016/j.coldregions.2024.104206, 2024.

238 Wen, H., Wu, X. Y., Liao, X., Wang, D., Huang, K. Y., and Wünnemann, B.: Application of machine learning methods
239 for snow avalanche susceptibility mapping in the Parlung Tsangpo catchment, southeastern Qinghai-Tibet Plateau, Cold
240 Regions Science and Technology, 198, 103535, https://doi.org/10.1016/j.coldregions.2022.103535, 2022.

241